

Nonlocal Flugge shell model for the axial buckling of single-walled Carbon nanotubes: An analytical approach

R. Ansari; H. Rouhi *

Department of Mechanical Engineering, University of Guilan, P.O. Box 3756, Rasht, Iran

Received 06 February 2015; revised 25 May 2015; accepted 10 June 2015; available online 30 July 2015

ABSTRACT: In this paper, the stability characteristics of single-walled carbon nanotubes (SWCNTs) under the action of axial load are investigated. To this end, a nonlocal Flugge shell model is developed to accommodate the small length scale effects. The analytical Rayleigh-Ritz method with beam functions is applied to the variational statement derived from the Flugge-type buckling equations. Through comparison of the results obtained from the present analytical solution and the ones from molecular dynamics (MD) simulations, the appropriate values of nonlocal parameter are proposed for (8, 8) armchair SWCNTs with different kinds of boundary conditions. The effects of nonlocal parameter and boundary conditions on the critical buckling load are also examined. Moreover, in spite of the uncertainty that exists in defining the in-plane stiffness and bending rigidity of nanotube, by adjusting the nonlocal parameter, the present nonlocal shell model is shown to be capable of predicting the MD simulations results.

Keywords: Axial buckling; Nonlocal elasticity; Rayleigh-Ritz method; Single-walled Carbon nanotube; Flugge shell.

INTRODUCTION

Notwithstanding the appearance of the first evidence for the tubular nature of carbon filaments in 1952 [1], the 1991 Iijima paper in Nature [2] re-ignited research interest in the scientific community of nanoscience and nanotechnology. This is largely due to the superior physical and chemical properties of carbon nanotubes (CNTs) over other existing materials. In terms of mechanical properties, CNTs have shown to be among the lightest, stiffest and strongest materials yet measured with high elastic modulus of greater than 1 TPa comparable to that of diamond and strengths many times higher than the strongest steel at a fraction of the weight. CNTs are expected to withstand large strains of up to 10% [3]. They are also quite flexible and can return to their original shape after bending and buckling [4].

The theoretical predictive models based on continuum mechanics are computationally efficient

and are gaining more popularity in recent years. Yao and Han [5] presented an elastic multi-shell model to study the buckling of multi-walled CNTs under torsional load coupling with temperature change. Based upon the finite-deformation shell theory, Lu *et al.* [6] studied the buckling of double-walled CNTs subjected to compression or torsion. On the basis of a continuum cylindrical shell model, buckling and post-buckling of multi-walled CNTs was investigated by He *et al.* [7]. Using a single-beam model, Ansari *et al.* [8] analyzed the thermal effect on nonlinear oscillations of CNTs with arbitrary boundary conditions. Also, there are many other researches in which the vibrational and buckling response of CNTs are studied via classical elasticity continuum [9-17].

One of the major drawbacks of the classical continuum mechanics, however, is that it is scale free and cannot accommodate size effects. As the dimensions of structures are scaled down to the submicron level, size effects become increasingly important. A more sophisticated version of continuum

✉ *Corresponding Author: Hessam Rouhi
Email: rouhi.hessam@gmail.com
Tel.: (+98) 13 33690276
Fax: (+98) 13 33690276

mechanics capable of accommodating size effects is the nonlocal continuum mechanics initiated by Eringen [18, 19]. The successful application of nonlocal continuum mechanics has been reported by many research workers [20-32]. These studies have been conducted based upon the beam models [21, 22, 26, 31], the shell models [23-25, 27, 29, 32] and the plate models [28, 30].

In the present work, a nonlocal shell model is developed based on the accurate Flügge shell theory to obtain the critical axial buckling load of SWCNTs. To analytically solve the problem, the Rayleigh-Ritz method is implemented to the variational form equivalent to the Flügge type stability equations. To derive the appropriate values of nonlocal parameter, the developed nonlocal model is calibrated with molecular dynamics (MD) simulation results. Due to the vagueness that exists in the specification of the proper values for the in-plane stiffness and bending rigidity of CNTs in the literature, the effects of these properties on the axial buckling behavior of SWCNTs are fully investigated in this paper.

EXPERIMENTAL

According to Eringen [18, 19], the concept of nonlocality is inherent in solid state physics where the nonlocal attractions of atoms are prevalent. Unlike the conventional elasticity theory, in the nonlocal continuum theory it is assumed that the stress at a point is a function of strains at all points in the continuum. The nonlocality is taken into account by applying the nonlocal constitutive equation given by Eringen [19]

$$(1 - (e_0 a)^2 \nabla^2) \sigma = \mathbf{t} \tag{1}$$

where \mathbf{t} is the macroscopic stress tensor at a point; $e_0 a$ is the nonlocal parameter or characteristic length which leads to consider the small scale effect; In the limit when the characteristic length goes to zero, the nonlocal elasticity reduces to the classical (local) elasticity. The stress tensor is related to the strain by generalized Hooke's law as

$$\mathbf{t} = \mathbf{S} : \boldsymbol{\varepsilon} \tag{2}$$

here \mathbf{S} is the fourth order elasticity tensor and $⋮$ denotes the double dot product. Hooke's law for the stress and strain relation is hence expressed by [19]

$$\begin{pmatrix} \sigma_{xx} \\ \sigma_{\theta\theta} \\ \sigma_{x\theta} \end{pmatrix} - (e_0 a)^2 \nabla^2 \begin{pmatrix} \sigma_{xx} \\ \sigma_{\theta\theta} \\ \sigma_{x\theta} \end{pmatrix} = \begin{pmatrix} \frac{E}{1-\nu^2} & \frac{\nu E}{1-\nu^2} & 0 \\ \frac{\nu E}{1-\nu^2} & \frac{E}{1-\nu^2} & 0 \\ 0 & 0 & \frac{E}{2(1+\nu)} \end{pmatrix} \begin{pmatrix} \varepsilon_{xx} \\ \varepsilon_{\theta\theta} \\ \gamma_{x\theta} \end{pmatrix} \tag{3}$$

Where E is Young's modulus of the material and ν is the Poisson's ratio. Also, x and θ are longitudinal and angular circumferential coordinates. σ_{xx} , $\sigma_{\theta\theta}$, and $\sigma_{x\theta}$ are normal and shear stresses and ε_{xx} , $\varepsilon_{\theta\theta}$, and $\gamma_{x\theta}$ are normal and shear strains. The Laplace operator in the polar coordinate system is given by $\nabla^2 = \partial^2 / \partial x^2 + \partial^2 / (R^2 \partial \theta^2)$, and R is the radius measured from the mid-plane of the cross section in the following CNT analysis.

Consider an elastic cylindrical shell of mid-plane radius R , length L , thickness h , as shown in Fig. 1. According to the classic shell theory, the three-dimensional displacement components u, v, w , and in the x, θ, z directions respectively are of the form [33]

$$\begin{aligned} u_x(x, \theta, z) &= u(x, \theta) - z \frac{\partial w}{\partial x}(x, \theta) \\ u_\theta(x, \theta, z) &= v(x, \theta) - z \frac{\partial w}{\partial \theta}(x, \theta) \\ u_z(x, \theta, z) &= w(x, \theta, z) \end{aligned} \tag{4}$$

where u, v, w are the reference surface displacements. The kinematic relations are given by [33]

$$\begin{pmatrix} \varepsilon_{xx} \\ \varepsilon_{\theta\theta} \\ \gamma_{x\theta} \end{pmatrix} = \begin{pmatrix} \frac{\partial u}{\partial x} \\ \frac{1}{R} \frac{\partial v}{\partial \theta} + \frac{w}{R} \\ \frac{\partial v}{\partial x} + \frac{1}{R} \frac{\partial u}{\partial \theta} \end{pmatrix} + z \begin{pmatrix} -\frac{\partial^2 w}{\partial x^2} \\ -\frac{1}{R^2} \left(\frac{\partial^2 w}{\partial \theta^2} + w \right) \\ -\frac{2}{R} \frac{\partial^2 w}{\partial x \partial \theta} + \frac{1}{R} \frac{\partial v}{\partial x} - \frac{1}{R^2} \frac{\partial u}{\partial \theta} \end{pmatrix} \tag{5}$$

The stress and moment resultants can be obtained by [33]

$$\begin{aligned} N &= (N_{xx}, N_{\theta\theta}, N_{x\theta})^T dz = \int_{-h/2}^{h/2} (\sigma_{xx}, \sigma_{\theta\theta}, \sigma_{x\theta})^T dz \\ M &= (M_{xx}, M_{\theta\theta}, M_{x\theta})^T dz = \int_{-h/2}^{h/2} (\sigma_{xx}, \sigma_{\theta\theta}, \sigma_{x\theta})^T z dz \end{aligned} \tag{6}$$

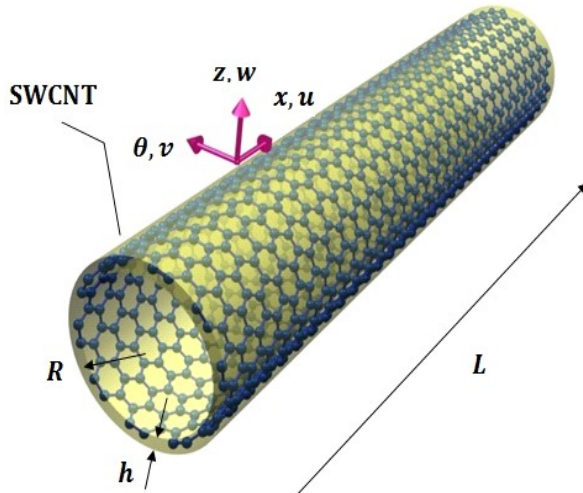


Fig. 1: Schematic of a single-walled carbon nanotube treated.

Moreover, in the nonlocal elastic shell theory, the stress and moment resultants are defined based on the stress components in equation (3), and therefore can be expressed as follows by using the kinematic relations in the Flügge shell theory [19,33]

$$\begin{pmatrix} N_{xx} \\ N_{\theta\theta} \\ N_{x\theta} \\ M_{xx} \\ M_{\theta\theta} \\ M_{x\theta} \end{pmatrix} - (e_0 a)^2 \nabla^2 \begin{pmatrix} N_{xx} \\ N_{\theta\theta} \\ N_{x\theta} \\ M_{xx} \\ M_{\theta\theta} \\ M_{x\theta} \end{pmatrix} = \begin{pmatrix} Eh \frac{\partial}{\partial x} & \frac{vEh}{R} \frac{1}{\partial \theta} & \frac{vEh}{R} \frac{1}{\partial \theta} \\ \frac{1-v^2}{R} \frac{\partial}{\partial x} & \frac{1-v^2}{R} \frac{\partial}{\partial \theta} & \frac{1-v^2}{R} \frac{\partial}{\partial \theta} \\ \frac{vEh}{R} \frac{\partial}{\partial x} & \frac{Eh}{R} \frac{1}{\partial \theta} & \frac{Eh}{R} \frac{1}{\partial \theta} \\ \frac{1-v^2}{R} \frac{\partial}{\partial x} & \frac{1-v^2}{R} \frac{\partial}{\partial \theta} & \frac{1-v^2}{R} \frac{\partial}{\partial \theta} \\ Eh \frac{1}{\partial \theta} & \frac{Eh}{R} \frac{\partial}{\partial x} & 0 \\ \frac{1}{2(1+\nu)} \frac{R}{\partial \theta} \frac{\partial}{\partial x} & \frac{1}{2(1+\nu)} \frac{\partial}{\partial x} & 0 \\ 0 & D \frac{v}{R^2} \frac{\partial}{\partial \theta} & -D \left(\frac{\partial^2}{\partial x^2} + \frac{v}{R^2} \frac{\partial^2}{\partial \theta^2} \right) \\ 0 & D \frac{1}{R^2} \frac{\partial}{\partial \theta} & -D \left(\frac{\partial^2}{\partial x^2} + \frac{1}{R^2} \frac{\partial^2}{\partial \theta^2} \right) \\ 0 & \frac{D}{R} (1-\nu) \frac{\partial}{\partial x} & -\frac{D}{R} (1-\nu) \frac{\partial^2}{\partial x \partial \theta} \end{pmatrix} \begin{pmatrix} u \\ v \\ w \end{pmatrix} \quad (7)$$

Where D is the bending rigidity of shell.

If x and θ denote the longitudinal and circumferential coordinates, respectively, the governing equations on the basis of the Flügge shell theory are given as [33]

$$\begin{aligned} \frac{\partial N_{xx}}{\partial x} + \frac{1}{R} \frac{\partial N_{\theta x}}{\partial \theta} &= P \frac{\partial^2 u}{\partial x^2} \\ \frac{1}{R} \frac{\partial N_{\theta\theta}}{\partial \theta} + \frac{\partial N_{x\theta}}{\partial x} + \frac{1}{R^2} \frac{\partial M_{\theta\theta}}{\partial \theta} + \frac{1}{R} \frac{\partial M_{x\theta}}{\partial x} &= P \frac{\partial^2 v}{\partial x^2} \\ \frac{\partial^2 M_{xx}}{\partial x^2} + \frac{1}{R^2} \frac{\partial^2 M_{\theta\theta}}{\partial \theta^2} + \frac{2}{R} \frac{\partial^2 M_{x\theta}}{\partial x \partial \theta} - \frac{N_{\theta\theta}}{R} &= P \frac{\partial^2 w}{\partial x^2} \end{aligned} \quad (8)$$

Where P represents the applied axial load.

By the use of equations (7), equations (8) can be stated in terms of the three field variables (u, v, w) as

$$\begin{aligned} l_{11}u + l_{12}v + l_{13}w &= Pu_{,xx} - (e_0 a)^2 \left[P \left(u_{,xxxx} + \frac{1}{R^2} u_{,\theta\theta\theta\theta} \right) \right] \\ l_{21}u + l_{22}v + l_{23}w &= Pv_{,xx} - (e_0 a)^2 \left[P \left(v_{,xxxx} + \frac{1}{R^2} v_{,\theta\theta\theta\theta} \right) \right] \\ l_{31}u + l_{32}v + l_{33}w &= Pw_{,xx} - (e_0 a)^2 \left[P \left(w_{,xxxx} + \frac{1}{R^2} w_{,\theta\theta\theta\theta} \right) \right] \end{aligned} \quad (9)$$

where l_{pq} ($p, q = 1, 2, 3$) are the partial operators, which are given in Appendix.

The Rayleigh-Ritz method is among the so-called variational approaches that are prevalently used in the analysis of continuous systems. In order to apply the Rayleigh-Ritz method, it is first necessary to obtain the variational statement equivalent to the partial differential equations that are governed by the buckling of SWCNTs.

According to the semi-inverse method [26], a variational trial-functional $\Pi(u, v, w)$ can be constructed as follows

$$\Pi(u, v, w) = \Pi_K(u, v, w) + \Pi_{Kg}(u, v, w) \quad (10)$$

in which

$$\begin{aligned} \Pi_K(u, v, w) &= \frac{1}{2} \int_0^L \int_{\Omega} \left(\left[\frac{Eh}{1-\nu^2} u_{,x} + \frac{vEh}{R(1-\nu^2)} (v_{,\theta} + w) \right] u_{,x} + \right. \\ &\quad \left. \frac{Eh}{2(1+\nu)} \left(\frac{u_{,\theta}}{R} + v_{,x} \right)^2 + \left[\frac{vEh}{1-\nu^2} u_{,x} + \frac{1}{R} \frac{Eh}{1-\nu^2} (v_{,\theta} + \right. \right. \\ &\quad \left. \left. w) \right] \frac{1}{R} (v_{,\theta} + w) + D(w_{,xx} + \frac{v}{R^2} w_{,\theta\theta}) w_{,xx} \right. \\ &\quad \left. + \frac{D}{R^2} \left(\left(\frac{1}{R^2} \right) w_{,\theta\theta} + \nu w_{,xx} \right) w_{,\theta\theta} + \frac{2(1-\nu)D}{R^2} (w_{,x\theta} - \right. \right. \\ &\quad \left. \left. - v_{,x})^2 - \frac{2D}{R^2} (\nu w_{,xx} + \frac{1}{R^2} w_{,\theta\theta}) v_{,\theta} \right) d\Omega dt \end{aligned} \quad (11)$$

and

$$\begin{aligned} \Pi_{Kg}(u, v, w) &= \frac{1}{2} \int_0^L \int_{\Omega} P \left((u_{,x})^2 - (e_0 a)^2 \left[\left(u_{,xx} + \frac{1}{R^2} u_{,\theta\theta} \right) u_{,xx} \right] + \right. \\ &\quad \left. (v_{,x})^2 - (e_0 a)^2 \left[\left(v_{,xx} + \frac{1}{R^2} v_{,\theta\theta} \right) v_{,xx} \right] + (w_{,x})^2 - \right. \\ &\quad \left. (e_0 a)^2 \left[\left(w_{,xx} + \frac{1}{R^2} w_{,\theta\theta} \right) w_{,xx} \right] \right) d\Omega dt \end{aligned} \quad (12)$$

The field variables of an SWCNT, i.e. u, v and w , are taken as

$$\begin{aligned} u &= A \frac{\partial \phi(x)}{\partial x} \cos(n\theta) \\ v &= B \phi(x) \sin(n\theta) \\ w &= C \phi(x) \cos(n\theta) \end{aligned} \quad (13)$$

Where A , B and C are the constant parameters, n the circumferential wave number and $\phi(x)$ is the axial function that satisfies the geometric boundary conditions of the CNT under consideration. The axial function $\phi(x)$ is selected as the characteristics beam function as [34]

$$\phi(x) = \alpha_1 \cosh\left(\frac{\lambda_m x}{L}\right) + \alpha_2 \cos\left(\frac{\lambda_m x}{L}\right) - \zeta_m \left[\alpha_3 \sinh\left(\frac{\lambda_m x}{L}\right) + \alpha_4 \sin\left(\frac{\lambda_m x}{L}\right) \right] \quad (14)$$

in which α_i ($i = 1, \dots, 4$) are constants with value 0, 1 or -1 depending on the tube ends, λ_m shows the roots of the transcendental equations obtained from the CNT boundary conditions and ζ_m denotes the parameters corresponding to . The parameters , and that are chosen according to the CNT boundary conditions are given in Table 1. Substituting equations (13) into equation (10) and then minimizing the energy functional with respect to the unknown coefficients , and result in the following algebraic equations

$$\frac{\partial \Pi}{\partial A} = 0, \quad \frac{\partial \Pi}{\partial B} = 0, \quad \frac{\partial \Pi}{\partial C} = 0 \quad (15)$$

The above equations can be recast in the form of a generalized eigenvalue problem. By solving the eigenvalue problem, the critical axial buckling loads of SWCNTs can be extracted and the associated eigenvectors yields the corresponding buckling mode shapes.

RESULTS AND DISCUSSION

In this section, the accuracy of the present solution is assessed first. Further several numerical results are presented to illustrate the buckling behavior of SWCNTs with SS, CC, CS and CF boundary conditions. The schematics of the considered end conditions are shown in Fig. 2. The mechanical properties and thickness of SWCNTs used in the numerical evaluations performed herein are taken to be $E=3.4\text{TPa}$, $\nu=0.3$, $D=0.85\text{ eV}$, $h=0.1\text{ nm}$ [32, 35-38], except otherwise stated.

Validation of the present approach by MD simulations results

In this subsection, the effectiveness of the present nonlocal shell model is assessed by MD simulations taken from [39] and the proper values of nonlocal parameter are proposed.

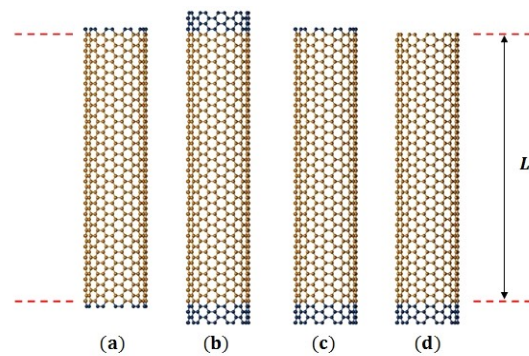


Fig. 2: Schematic of SWCNTs with (a) SS, (b) CC, (c) CS and (d) CF end conditions.

The critical axial buckling loads of simply-supported, clamped-free and clamped (8,8) armchair SWCNTs versus nanotube aspect ratio (L/d) are plotted in Figs. 3 and 4. To make the model more realistic, the nonlocal parameter $e_0 a$ needs to be calibrated such that the nonlocal shell model predicts the results of MD simulations. The least-square method is used to determine the best value for the nonlocal parameter so that the sum of the squares of the errors between the results from MD simulations and the corresponding ones from the nonlocal shell model is minimized for a relatively large range of . From these figures, the nonlocal shell model developed herein is capable of predicting the results of MD simulations provided that the nonlocal parameter is properly calibrated. The values of the nonlocal parameter are, and, corresponding to the simply-supported, clamped-free and clamped SWCNTs, respectively. This indicates that the significance of the small size effects on the critical buckling loads of SWCNTs is dependent on the boundary conditions of CNT. As shown in Figs. 3 and 4, the local shell model ($e_0 a=0$) tends to overestimate the critical buckling loads of SWCNT, especially when its aspect ratio decreases. In addition, Fig. 4 shows that as the small-scale parameter increases, the critical buckling load obtained from the nonlocal shell model becomes smaller than that from its local counterpart.

Illustrative examples

Example 1: In this example, a comparison is made between the results calculated by the present Flügge shell model and those computed from the Donnell shell model developed in [39]. The values of critical buckling loads corresponding to SWCNTs with different end

conditions calculated based upon the MD simulations and nonlocal continuum theory including the Donnell and Flugge shell models are tabulated in Table 2. It is observed that the results generated by the Flugge shell model are in closer agreement with the ones computed via MD simulations.

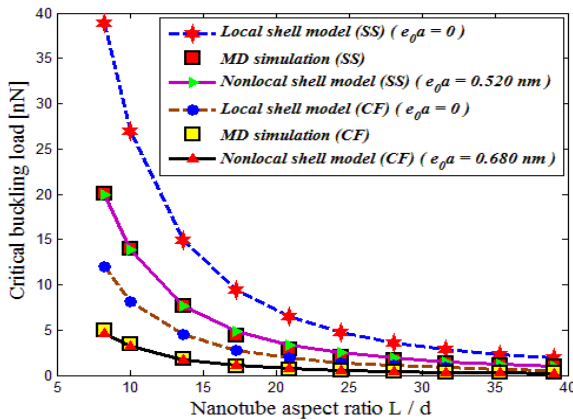


Fig. 3: Critical axial buckling loads from continuum shell model and MD simulation for (8,8) armchair simply-supported and clamped-free SWCNTs.

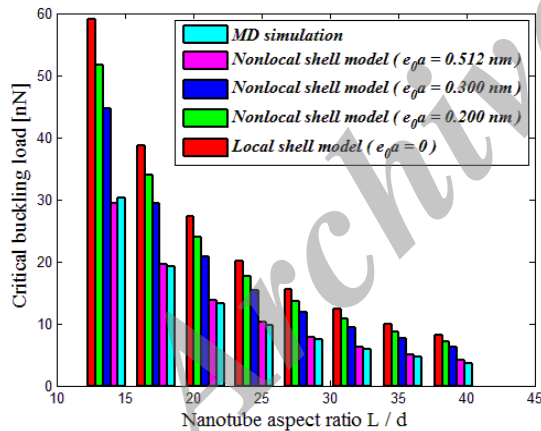


Fig. 4: Critical axial buckling loads from continuum shell model and MD simulations for (8,8) armchair clamped SWCNTs.

From Table 2, at higher values of aspect ratio where the effect of nonlocality diminishes, the Donnell shell model tends to overestimate the critical buckling loads of nanotubes. This reveals that in the buckling analysis of SWCNTs, applying the Flugge shell theory increases the accuracy of the results as compared to the corresponding Donnell one. From this table, for the

case of clamped boundary conditions, at lower values of aspect ratio (i.e. $L/d = 6.5, 8.3$ and 10.1) the difference between the results of the nonlocal shell models and those of MD simulations becomes more pronounced. Furthermore, for all the selected boundary conditions, the values of nonlocal parameter related to the Flugge shell model are lower than those of Donnell shell model.

Example 2: Presented graphically in Fig. 5 is the critical buckling load of a simply supported SWCNT versus a wide range of its aspect ratio L/R for several nonlocal parameters. The values of the nonlocal parameter are assumed to be varied from $e_0 a = 0$ (corresponding to the classical/ local continuum model) to $e_0 a = 2 \text{ nm}$. According to this figure, two types of buckling are readily distinguishable: the shell-like buckling which is almost independent of nanotube aspect ratio and the column-like buckling which is strongly sensitive to the aspect ratio. For CNTs of relatively short length for which the shell-like buckling is dominant, the profound effects of the small length scale on the critical buckling loads of the CNT are seen from Fig. 5, especially for shorter CNTs and higher values of nonlocal parameter. As the aspect ratio increases, the effect of small length scale diminishes so that the buckling envelopes tend to converge. In other words, the critical buckling loads of long CNTs for which the column-like buckling becomes dominant are insensitive to the effect of the small length scale. Unlike the classical continuum model, the present nonlocal shell model is capable of predicting the strong dependence of the critical buckling loads on nanotube aspect ratio whether short or long.

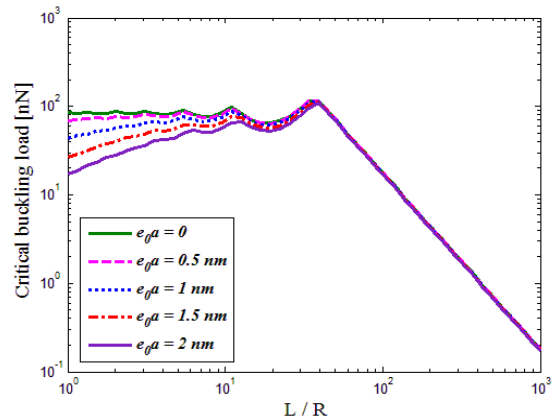


Fig. 5: Effect of the nonlocal parameter on the critical buckling load for a simply-supported SWCNT ($R = 8.5 \text{ nm}$).

Table 1: Values of α_i , λ_m and ζ_m for SS, CC, FF, CS, CF and FS boundary conditions.







Boundary condition	$\alpha_i (i = 1, \dots, 4)$	λ_m	ζ_m
 SS	$\alpha_1 = 0, \alpha_2 = 0$ $\alpha_3 = 0, \alpha_4 = -1$	$m\pi$	1
 CC	$\alpha_1 = 1, \alpha_2 = -1$ $\alpha_3 = 1, \alpha_4 = -1$	$\cos\lambda_m \cosh\lambda_m = 1$	$\frac{\cosh\lambda_m - \cos\lambda_m}{\sinh\lambda_m - \sin\lambda_m}$
 FF	$\alpha_1 = 1, \alpha_2 = 1$ $\alpha_3 = 1, \alpha_4 = 1$	$\cos\lambda_m \cosh\lambda_m = 1$	$\frac{\cosh\lambda_m - \cos\lambda_m}{\sinh\lambda_m - \sin\lambda_m}$
 CS	$\alpha_1 = 1, \alpha_2 = -1$ $\alpha_3 = 1, \alpha_4 = -1$	$\tan\lambda_m = \tanh\lambda_m$	$\frac{\cosh\lambda_m - \cos\lambda_m}{\sinh\lambda_m - \sin\lambda_m}$
 CF	$\alpha_1 = 1, \alpha_2 = -1$ $\alpha_3 = 1, \alpha_4 = -1$	$\cos\lambda_m \cosh\lambda_m = -1$	$\frac{\sinh\lambda_m - \sin\lambda_m}{\cosh\lambda_m + \cos\lambda_m}$
 FS	$\alpha_1 = 1, \alpha_2 = 1$ $\alpha_3 = 1, \alpha_4 = 1$	$\tan\lambda_m = \tanh\lambda_m$	$\frac{\cosh\lambda_m - \cos\lambda_m}{\sinh\lambda_m - \sin\lambda_m}$

Table 2: Critical buckling loads [nN] of (8,8) armchair SWCNTs with different boundary conditions calculated by the MD simulations and nonlocal continuum models.

Boundary condition	Critical buckling load (nN)	L/d										
		6.5	8.3	10.1	13.7	17.3	20.9	24.5	28.1	31.6	35.3	39.1
SS	P_{cr}^a	31.4797	20.1078	13.9871	7.6032	4.3763	2.9126	2.0916	1.7015	1.3669	1.1504	0.9873
	P_{cr}^b ($e_0 a = 0.540$ nm)	30.0646	19.4915	13.6406	7.7084	4.9875	3.5284	2.6499	2.0891	1.7056	1.4235	1.2169
	P_{cr}^c ($e_0 a = 0.520$ nm)	30.9614	19.9627	13.8808	7.7173	4.8912	3.3760	2.4637	1.8814	1.4833	1.1904	0.9758
CC	P_{cr}^a	97.4455	78.1883	54.3710	30.0112	18.0081	12.3350	9.1807	7.1938	5.7207	4.6297	3.8385
	P_{cr}^b ($e_0 a = 0.531$ nm)	76.7331	63.3080	48.2690	29.6402	19.7522	14.0570	10.4870	8.1507	6.5266	5.3180	4.4250
	P_{cr}^c ($e_0 a = 0.512$ nm)	79.2345	65.4812	49.8126	30.4480	20.1848	14.2775	10.5760	8.1541	6.4708	5.2183	4.2929
CS	P_{cr}^a	37.819	40.1430	27.9077	15.4001	9.0556	6.1014	4.5348	3.6476	2.8996	2.3552	1.9582
	P_{cr}^b ($e_0 a = 0.550$ nm)	52.0678	36.9465	26.6993	15.5049	10.0879	7.1075	5.2872	4.1149	3.3087	2.7133	2.2757
	P_{cr}^c ($e_0 a = 547$ nm)	52.0126	36.9085	26.5928	15.3266	9.8757	6.8769	5.0455	3.8662	3.0551	2.4560	2.0158
CF	P_{cr}^a	7.3406	4.9448	3.4483	1.8522	1.0359	0.6760	0.4990	0.3807	0.3236	0.2814	0.2416
	P_{cr}^b ($e_0 a = 0.722$ nm)	7.0698	4.4885	3.1323	1.8036	1.2087	0.8932	0.7045	0.5845	0.5026	0.4425	0.3985
	P_{cr}^c ($e_0 a = 0.680$ nm)	7.4101	4.6255	3.1627	1.7299	1.0885	0.7484	0.5449	0.4155	0.3273	0.2625	0.2150

^a Calculated based on MD simulations

^b Calculated based on the Dönnell shell model

^c Calculated based on the Flügge shell model

Example 3: For the results generated so far, the nanotube in-plane stiffness Eh has been taken to be 340 Jm^{-2} . However, there exist some inconsistencies concerning this quantity in the literature. The reported CNT in-plane stiffness is largely scattered, ranging from 300 to 420 Jm^{-2} [40]. Figs. 6(a)-6(d) are presented to investigate the influence of the in-plane stiffness variation on the critical buckling loads of a (8,8) armchair

SWCNT with SS, CC, CS and CF boundary conditions, respectively. This figure shows that for all the selected boundary conditions, the critical buckling loads calculated via the local shell model are sensitive to the nanotube in-plane stiffness and also the larger the in-plane stiffness, the higher the critical buckling loads. The difference is more considerable for shorter length CNTs. However, regardless of the ambiguity

that exists in defining nanotube in-plane stiffness, via calibrating the nonlocal parameter, the present nonlocal shell model is capable of predicting the MD simulations results. Table 3 presents the critical buckling loads corresponding to SWCNTs with simply-supported end conditions for two different values of in-plane stiffness. As can be seen in this table, in contrast to the local shell model, even in the presence of uncertainty in defining the in-plane stiffness, the nonlocal shell model has the potential to predict the MD simulations results provided that the nonlocal parameter is appropriately adjusted.

Example 4: Previous study reveals that the bending rigidity of SWCNTs should be regarded as an independent material parameter not related to the representative thickness by the classic bending rigidity formula, i.e. $D = Eh^3/12(1 - \nu^2)$, and the actual bending rigidity of SWCNTs is lower than its classical counterpart [41]. Thus, due to the not-well-defined

nanotube bending rigidity, the critical buckling loads of simply supported and clamped-free SWCNTs with bending rigidity of and against the ratio are tabulated in Table 4. It is observed that applying the bending rigidity of to the local continuum shell model, yields the slight increase of the critical buckling loads. For the nonlocal shell model with bending rigidity of to be in agreement with the MD simulations results, the values of the nonlocal parameter are and , corresponding to the simply supported and clamped-free SWCNTs, respectively, which are a little higher than those corresponding to SWCNTs with bending rigidity of .

The three dimensional buckling mode shapes of a simply supported SWCNT are plotted in Fig. 7(a-d), for which the circumferential mode number is considered to be 5 and axial mode number varies from 1 to 4. These figures are also accompanied by a cross-sectional view in the middle of the SWCNT.

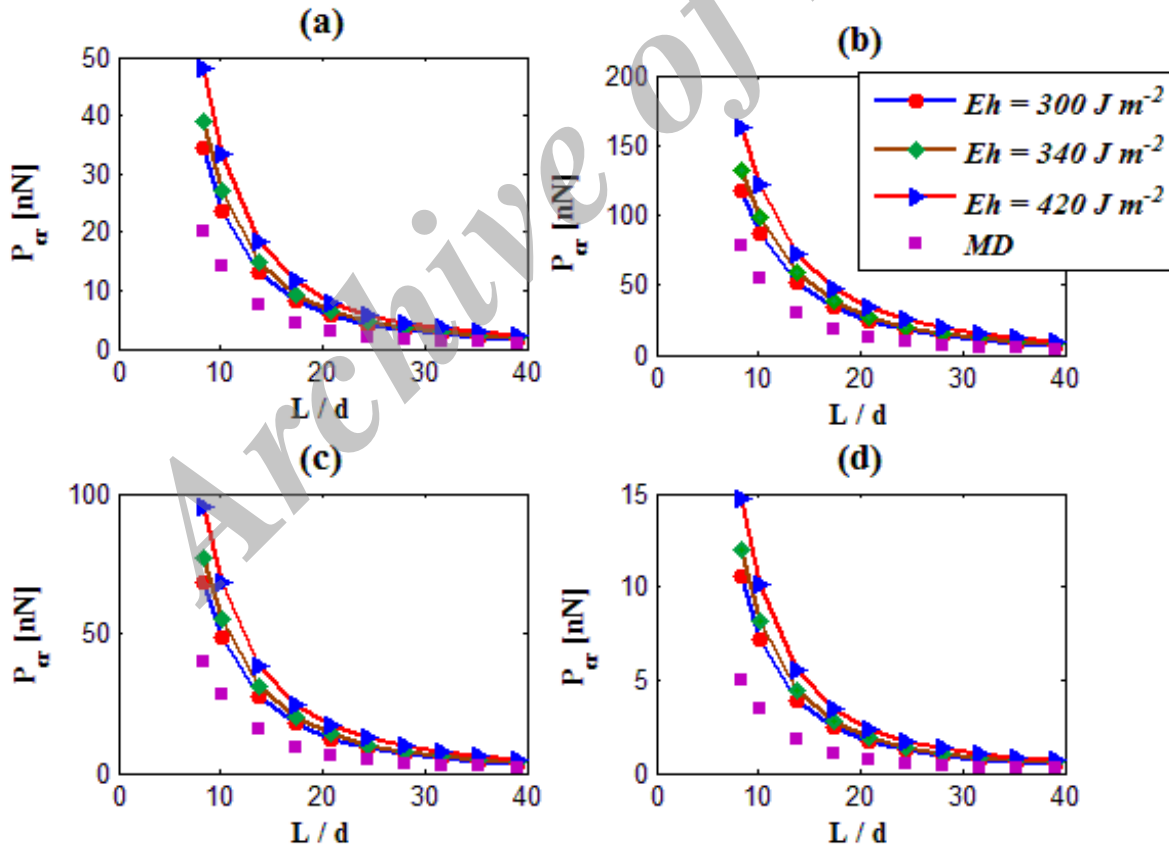


Fig. 6: Influence of the in-plane stiffness on the critical buckling load of a (8,8) armchair SWCNT ($e_0 a = 0$) with: (a) simply supported-simply supported, (b) clamped-clamped, (c) clamped-simply supported, (d) clamped-free boundary conditions.

Table 3: Critical buckling loads [nN] of (8,8) armchair simply-supported SWCNTs for different values of in-plane stiffness.

L/d	MD simulations	Nonlocal shell model ($Eh = 300 \text{ J m}^{-2}, e_0 a = 0.451 \text{ nm}$)	Nonlocal shell model ($Eh = 420 \text{ J m}^{-2}, e_0 a = 0.633 \text{ nm}$)
6.5	31.4797	31.1260	30.8971
8.3	20.1078	20.0376	19.9643
10.1	13.9871	13.9217	13.8974
13.7	7.6032	7.7340	7.7349
17.3	4.3763	4.9001	4.9047
20.9	2.9126	3.3815	3.3861
24.5	2.0916	2.4675	2.4715
28.1	1.7015	1.8842	1.8876
31.6	1.3669	1.4853	1.4882
35.3	1.1504	1.1920	1.1944
39.1	0.9873	0.9771	0.9791

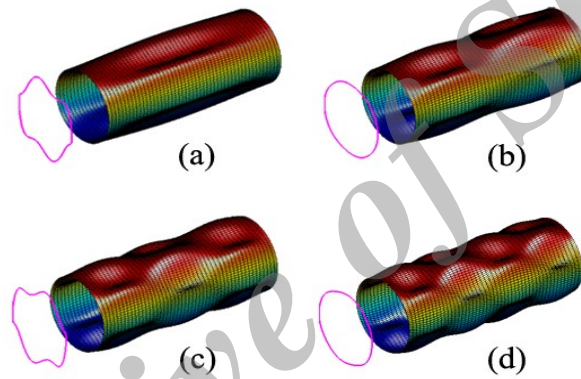


Fig. 7: Buckling mode shapes of a simply-supported SWCNT in the fifth circumferential mode number ($R=8.5 \text{ nm}, L/R=5$): (a) first axial mode, (b) second axial mode, (c) third axial mode, (d) fourth axial mode.

Table 4: Critical buckling loads [nN] of a (8,8) armchair SWCNT with simply supported-simply supported and clamped-free boundary conditions for different values of bending rigidity.

L/d	SS				CF			
	Local shell model ($e_0 a = 0$) $D = 0.85 \text{ eV}$	Local shell model ($e_0 a = 0$) $D = \frac{Eh^3}{12(1-\nu^2)}$	Nonlocal shell model ($e_0 a = 0.524$) $D = \frac{Eh^3}{12(1-\nu^2)}$	MD	Local shell model ($e_0 a = 0$) $D = 0.85 \text{ eV}$	Local shell model ($e_0 a = 0$) $D = \frac{Eh^3}{12(1-\nu^2)}$	Nonlocal shell model ($e_0 a = 0.682$) $D = \frac{Eh^3}{12(1-\nu^2)}$	MD
6.5	61.0513	61.1796	30.7921	31.4797	19.2250	19.2588	7.3966	7.3406
8.3	38.9430	39.0194	19.8525	20.1078	11.9552	11.9755	4.6167	4.9448
10.1	26.9300	26.9810	13.8038	13.9871	8.1588	8.1724	3.1566	3.4483
13.7	14.8932	14.9203	7.6743	7.6032	4.4545	4.4618	1.7265	1.8522
17.3	9.4172	9.4341	4.8639	4.3763	2.8006	2.8051	1.0863	1.0359
20.9	6.4918	6.5034	3.3571	2.9126	1.9248	1.9279	0.7469	0.6760
24.5	4.7341	4.7425	2.4500	2.0916	1.4011	1.4034	0.5438	0.4990
28.1	3.6135	3.6199	1.8709	1.7015	1.0682	1.0699	0.4147	0.3807
31.6	2.8479	2.8529	1.4750	1.3669	0.8412	0.8426	0.3266	0.3236
35.3	2.2850	2.2890	1.1837	1.1504	0.6746	0.6756	0.2619	0.2814
39.1	1.8728	1.8761	0.9703	0.9873	0.5526	0.5535	0.2146	0.2416

CONCLUSION

Based upon the Eringen theory of nonlocal elasticity, the stability characteristics of SWCNTs subjected to the axial load were analyzed. The variational form of the Flügge type buckling equations was constructed to which the Rayleigh-Ritz method was applied. Among the more significant conclusions to be obtained, the following findings may be summarized from the present study:

The present theoretical formulation based on the Flügge shell theory is simpler and more accurate than those based on the Donnell shell theory. The classical continuum model tends to overestimate the critical buckling loads of small size nanotubes and one must recourse to the nonlocal version to reduce the relative error. As the small-scale parameter increases, the critical buckling loads obtained from the nonlocal shell model become smaller than those from its local counterpart. The effects of small length scale on the critical buckling load are more pronounced for SWCNTs of relatively short length for which the shell-like buckling is dominant. However, the critical buckling loads of long CNTs for which the column-like buckling becomes dominant are insensitive to the effect of the small length scale. The significance of the small size effects on the critical buckling loads of SWCNTs was shown to be dependent on geometric parameters, boundary conditions and material properties of SWCNT. In spite of the uncertainty that exists in defining nanotube in-plane stiffness and bending rigidity, by adjusting the nonlocal parameter, the present nonlocal shell model was shown to be capable of predicting the MD simulations results.

Appendix

$$l_{11} = \frac{Eh}{1-\nu^2} \frac{\partial^2}{\partial x^2} + \frac{1}{R^2} \frac{Eh}{2(1+\nu)} \frac{\partial^2}{\partial \theta^2}$$

$$l_{12} = \frac{1}{R} \left(\frac{Eh\nu}{1-\nu^2} + \frac{Eh}{2(1+\nu)} \right) \frac{\partial^2}{\partial x \partial \theta}$$

$$l_{13} = \frac{1}{R} \frac{E\nu h}{1-\nu^2} \frac{\partial}{\partial x}$$

$$l_{21} = l_{12}$$

$$l_{22} = \left(\frac{Eh}{2(1+\nu)} + \frac{D}{R^2} (1-\nu) \right) \frac{\partial^2}{\partial x^2} + \frac{1}{R^2} \left(\frac{Eh}{1-\nu^2} + \frac{D}{R^2} \right) \frac{\partial^2}{\partial \theta^2}$$

$$l_{23} = -\frac{D}{R^2} \frac{\partial^3}{\partial x^2 \partial \theta} - \frac{\nu D}{R^4} \frac{\partial^3}{\partial \theta^3} + \frac{1}{R^2} \frac{Eh}{1-\nu^2} \frac{\partial}{\partial \theta}$$

$$l_{31} = -l_{13}$$

$$l_{32} = \frac{D}{R^2} (2-\nu) \frac{\partial^3}{\partial x^2 \partial \theta} + \frac{D}{R^4} \frac{\partial^3}{\partial \theta^3} - \frac{1}{R^2} \frac{Eh}{1-\nu^2} \frac{\partial}{\partial \theta}$$

REFERENCES

- [1] Radushkevich L. V., and Lukyanovich V. M., (1952), O strukture ugleroda, Obrazujucesja pri termiceskom razlozenii okisi ugleroda na zeleznom kontakte. *Zurn. Fisic. Chim.* 26: 88-95.
- [2] Iijima S., (1991), Helical Microtubes of Graphitic Carbon, *Nature* (London), 354: 56-58.
- [3] Nardelli M. B., Bernholc J., (1999), Mechanical Deformations and Coherent Transport in Carbon Nanotubes. *Phys. Rev. B.* 60: 16338-16341.
- [4] Falvo M. R., Clary G. J., Taylor R. M., Chi V., Brooks F. P., Washburn S., Superfine R., (1997), Bending and buckling of carbon nanotubes under large strain. *Nature.* 389: 582-584.
- [5] Yao X., Han, Q., (2006), Buckling Analysis of Multiwalled Carbon Nanotubes Under Torsional Load Coupling With Temperature Change. *ASME. J. Eng. Mater. Technol.* 128: 419-427.
- [6] Lu W. B., Wu J., Feng X., Hwang K. C., Huang Y., (2010), Buckling Analyses of Double-Wall Carbon Nanotubes: A Shell Theory Based on the Interatomic Potential. *ASME. J. Appl. Mech.* 77: 061016-19.
- [7] He X. Q., Kitipornchai S., Wang C. M., Xiang Y., Zhou Q., (2010), A Nonlinear Van Der Waals Force Model for Multiwalled Carbon Nanotubes Modeled by a Nested System of Cylindrical Shells. *ASME. J. Appl. Mech.* 77: 061006-11.
- [8] Ansari R., Hemmatnezhad M., Rezapour J., (2011), The Thermal Effect on Nonlinear Oscillations of Carbon Nanotubes with Arbitrary Boundary Conditions. *Curr. Appl. Phys.* 11: 692-697.
- [9] Pantano A., Boyce M. C., Parks D. M., (2004), Mechanics of Axial Compression of Single and Multi-Wall Carbon Nanotubes. *ASME. J. Eng. Mater. Technol.* 126: 279-284.
- [10] Behfar K., Naghdabadi R., (2005), Nanoscale Vibrational Analysis of a Multi-Layered Graphene Sheet Embedded in an Elastic Medium. *Compos. Sci. Technol.* 65: 1159-1164.
- [11] Han Q., Yao X., Li L., (2006), Theoretical and Numerical Study of Torsional Buckling of Multiwall Carbon Nanotubes. *Mech. Adv. Mater. Struct.* 13: 329-337.
- [12] Wang C. M., Tan V. B. C., Zhang Y. Y., (2006), Timoshenko Beam Model for Vibration Analysis of Multi-Walled Carbon Nanotubes. *J. Sound Vib.* 294: 1060-1072.
- [13] Dong K., Liu B. Y., Wang X., (2008), Wave Propagation in Fluid-Filled Multi-Walled Carbon Nanotubes Embedded in Elastic matrix. *Comput. Mater. Sci.* 42: 139-148.
- [14] Wang L., Ni Q., Li M., Qian Q., (2008), The Thermal Effect on Vibration and Instability of Carbon Nanotubes Conveying Fluid. *Physica E.* 40: 3179-3182.
- [15] Ansari R., Hemmatnezhad M., Ramezannezhad H., (2009), Application of HPM to the Nonlinear Vibrations of Multiwalled Carbon Nanotubes. *Numer. Meth. Part. D. E.* 26: 490-500.
- [16] Ansari R., Rouhi S., (2010), Atomistic Finite Element Model for Axial Buckling of Single-Walled Carbon Nanotubes. *Physica E.* 43: 58-69.
- [17] Ansari R., Hemmatnezhad M., (2011), Nonlinear Vibrations of Embedded Multiwalled Carbon Nanotubes Using a Variational Approach. *Math. Comput. Model.* 53: 927-38.
- [18] Eringen A. C., (1983), On Differential Equations of Nonlocal Elasticity and Solutions of Screw Dislocation and Surface Waves. *J. Appl. Phys.* 54: 4703-4710.
- [19] Eringen A. C., (2002), *Nonlocal Continuum Field Theories*, Springer, New York.

- [20] Peddieson J., Buchanan G. R., McNitt R. P., (2003), Application of Nonlocal Continuum Models to Nanotechnology. *Int. J. Eng. Sci.* 41: 305-312.
- [21] Sudak L. J., (2003), Column Buckling of Multiwalled Carbon Nanotubes Using Nonlocal Continuum Mechanics. *J. Appl. Phys.* 94: 7281-7287.
- [22] Wang Q., Varadan V. K., (2006), Vibration of Carbon Nanotubes Studied Using Nonlocal Continuum Mechanics. *Smart Mater. Struct.* 15: 659-666.
- [23] Wang Q., Wang C. M., (2007), The Constitutive Relation and Small Scale Parameter of Nonlocal Continuum Mechanics for Modeling Carbon Nanotubes. *Nanotech.* 18: 075702.
- [24] Li R., Kardomateas G. A., (2007), Thermal Buckling of Multi-Walled Carbon Nanotubes by Nonlocal Elasticity. *ASME. J. Appl. Mech.* 74: 399-405.
- [25] Hu Y. G., Liew K. M., Wang Q., He X. Q., Yakobson, B. I., (2008), Nonlocal Shell Model for Elastic Wave Propagation in Single- and Double-Walled Carbon Nanotubes. *J. Mech. Phys. Solids.* 56: 3475-3485.
- [26] Adali S., (2008), Variational Principles for Multi-Walled Carbon Nanotubes Undergoing Buckling Based on Nonlocal Elasticity Theory. *Phys. Lett. A.* 372: 5701-5705.
- [27] Shen H. S., Zhang C. L., (2010), Nonlocal Shear Deformable Shell Model for Post-Buckling of Axially Compressed Double-Walled Carbon Nanotubes Embedded in an Elastic Matrix. *ASME. J. Appl. Mech.* 77: 041006.
- [28] Ansari R., Rajabiehfarid R., Arash B., (2010), Nonlocal Finite Element Model for Vibrations of Embedded Multi-Layered Graphene Sheets. *Comput. Mater. Sci.* 49: 831-838.
- [29] Arash B., Ansari, R., (2010), Evaluation of Nonlocal Parameter in the Vibrations of Single-Walled Carbon Nanotubes with Initial Strain. *Physica E.* 42: 2058-2064.
- [30] Ansari R., Sahmani S., Arash B., (2010), Nonlocal Plate Model for Free Vibrations of Single-Layered Graphene Sheets. *Phys. Lett. A.* 375: 53-62.
- [31] Ansari R., Faghieh Sh. M., Mohammadi V., Gholami R., Rouhi H., (2015), Buckling and Postbuckling of Single-Walled Carbon Nanotubes Based on a Nonlocal Timoshenko Beam Model. *ZAMM.* 95: 939-951.
- [32] Ansari R., Rouhi H., (2011), Analytical Treatment of the Free Vibration of Single-Walled Carbon Nanotubes Based on the Nonlocal Flügge Shell Theory *ASME. J. Eng. Mater. Technol.* 134: 011008-011016.
- [33] Flügge W., (1960), Stresses in Shells, *Springer*, Berlin.
- [34] Loy C., T., Lam K., Y., (1997), Vibration of Cylindrical Shells with Ring Support. *Int. J. Mech. Sci.* 39: 445-471.
- [35] Batra R. C., Gupta S. S., (2008), Wall Thickness and Radial Breathing Modes of Single-Walled Carbon Nanotubes. *ASME. J. Appl. Mech.* 75: 061010-14.
- [36] Wang C. Y., Zhang L. C., (2008), An Elastic Shell Model for Characterizing Single-Walled Carbon Nanotubes. *Nanotechnol.* 19: 195704-09.
- [37] Yakobson B. I., Brabec C. J., Bernholc J., (1996), Nanomechanics of Carbon Tubes: Instability Beyond Linear Response. *Phys. Rev. Lett.* 76: 2511-2514.
- [38] Yan Y., Wang W. Q., Zhang L. X., (2010), Nonlocal Effect on Axially Compressed Buckling of Triple-Walled Carbon Nanotubes Under Temperature Field. *Appl. Math. Model.* 34: 3422-3429.
- [39] Ansari R., Sahmani S., Rouhi H., (2011), Rayleigh-Ritz Axial Buckling Analysis of Single-Walled Carbon Nanotubes with Different Boundary Conditions. *Phys. Lett. A.* 375: 1255-1263.
- [40] Wang C. Y., Zhang L. C., (2008), A Critical Assessment of the Elastic Properties and Effective Wall Thickness of Single-Walled Carbon Nanotubes. *Nanotechnol.* 19: 075705.
- [41] Ru C. Q., (2000), Effective Bending Stiffness of Carbon Nanotubes. *Phys. Rev. B.* 62: 9973-9976.

How to cite this article: (Vancouver style)

Ansari R., Rouhi H., (2015), Nonlocal Flugge shell model for the axial buckling of single-walled Carbon nanotubes: An analytical approach. *Int. J. Nano Dimens.* 6(5): 453-462.
 DOI: [10.7508/ijnd.2015.05.002](https://doi.org/10.7508/ijnd.2015.05.002)
 URL: http://ijnd.ir/article_15160_1117.html